ACS APPLIED MATERIALS & INTERFACES

Research Article

www.acsami.org

Multifunctional Fe_3O_4@P(St/MAA)@Chitosan@Au Core/Shell Nanoparticles for Dual Imaging and Photothermal Therapy

Xuandong Wang,[†,‡] Huiyu Liu,[†] Dong Chen,[†] Xianwei Meng,[†] Tianlong Liu,[†] Changhui Fu,[†] Nanjing Hao,[†,‡] Yanqi Zhang,[†] Xiaoli Wu,[†,‡] Jun Ren,*[,†] and Fangqiong Tang*[,†]

[†]Laboratory of Controllable Preparation and Application of Nanomaterials, Technical Institute of Physics and Chemistry, Chinese Academy of Sciences, Beijing 100190, People's Republic of China

[‡]University of the Chinese Academy of Sciences, Beijing 100049, People's Republic of China

Supporting Information

ABSTRACT: Merging different components into a single nanoparticle can exhibit profound impact on various biomedical applications including diagnostics, imaging, and therapy. However, retaining the unique properties of each component after integration has proven to be a significant challenge. Our previous research demonstrated that gold nanoshells on polystyrene spheres have potential in photohermal therapy. Here, we report a facile and green strategy to synthesize a multifunctional nanocomposite with Fe_3O_4 core coated gold nanoshells as dual imaging probes and photothermal agents. The as-prepared nanoparticles exhibit well-defined structure and excellent physical properties such as magnetic and plasmonic activities. Therefore, they were applied as contrast agents in magnetic resonance imaging (MRI) and dark field imaging (DFI). Besides, we demonstrated their potential application in photothermal therapy. Moreover, the obtained multifunctional nanoparticles have shown excellent biocompatibility for their low cytotoxicity and hemolyticity.

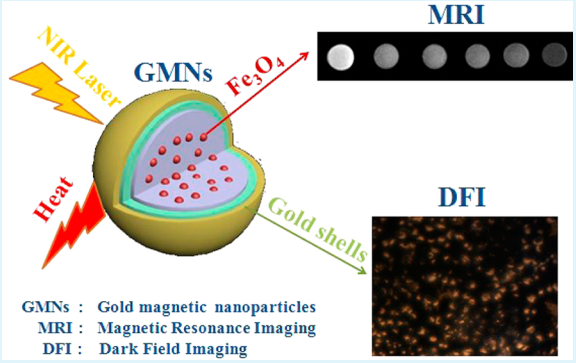

KEYWORDS: *magnetic cores, gold nanoshells, magnetic resonance imaging (MRI), dark field imaging (DFI), photothermal therapy*

1. INTRODUCTION

In recent years, multifunctional nanoparticles (NPs) with various components have attracted intensive interest because they show superior properties than that of the individual component. Among the various functional nanomaterials, magnetic nanoparticles (MNPs) have a broad application in magnetic fluids,[1] catalysis,[2] magnetic bioseparation,[3] hyperthermia,[4,5] and drug delivery.[6] In particular, MNPs can be used as a high performance T 2-weighted magnetic resonance imaging (MRI) contrast agent owing to their deep tissue penetration and high resolution.[7] They could also be ultilized together with fluorescent dyes,[8] up-conversion nanoparticles,[9] quantum dots,[10] or plasmonic nanocrystals[11−13] for multimodal imaging applications. Among those functional components coupling with MNPs, gold nanomaterials seem to be good candidates due to their excellent biocompatibility and stability, easy synthesis, and surface modification. The strong light scattering property of Au NPs also makes them powerful dark field imaging (DFI) contrast agents.[14] Furthermore, as discussed in our previous studies and other reports, gold nanoshells can be used as good photothermal agents in vivo.[15−17] Coating gold nanoshells onto magnetic nanoparticles endows them the unique magnetic and optical properties but also ensures their biocompatibility, especially for photothermal therapy, which facilitates their bioapplications of MNPs. Therefore, more and more scientists focus on the research of synthesis and application of gold magnetic nanocomposites.[18]

In general, there are two strategies to synthesize the multifunctional nanocomposites comprising magnetic core and gold nanoshells.[19,20] The first one is to directly coat gold nanoshells onto iron oxide nanoparticles.[19] Although it is a simple and saving strategy, NPs usually tend to form agglomeration during the coating process and have unfortunate results in decreasing the saturation magnetization of MNPs, losing potential applications for near-infrared resonance (NIR) optical absorption property of gold nanoshells. The other strategy generally used is using a silica[21] or polymer[20,22] middle layer as the bridge of the magnetic core and the outer gold nanoshells. In a recent attempt, the polymer as the middle layer has also been developed. Hsiao's group prepared magnetic nanoparticles by a hydrothermal method, followed by the polymerization of styrene and methyl methacrylate onto the Fe_3O_4 and self-reduction of gold on the outer layer of the particles.[23] However, it was hard to get continuous gold nanoshells onto the surface of the polymer with the self-

Received: February 26, 2013
Accepted: May 17, 2013
Published: May 17, 2013

reduction method, which may affect the NIR absorption in photothermal therapy.

To overcome the above problems, herein, on the basis of the work of our group's strategy of coating gold nanoshells on the surface of the carboxylated polystyrene sphere,[24] we report a novel method using Fe_3O_4 within carboxylated polystyrene sphere as the core; chitosan (CHI) was used to modify the surface of the polymer sphere for further attachment of gold colloids. CHI has been used as an excellent modification molecule because of its biocompatibility, biodegradability, and bioactivity.[25,26] On one hand, the polymer can prevent a direct contact of the gold nanoshells and magnetic particles, while not reducing the magnetic field strength so fast like other reports. On the other hand, the polymer layer could decrease agglomeration during the coating process. Furthermore, the Fe_3O_4 cores of the obtained nanoparticles facilitate magnetic field guided movement and MRI imaging. In addition, the gold nanoshells can be used as DFI contrast agents and for photothermal therapy of cancer cells. The combined functionalities have a great potential in biomedical applications, which show a powerful way for personalized treatment of diseases.

2. EXPERIMENTAL SECTION

2.1. Materials. Oleic acid (OA), ferric chloride hexahydrate ($FeCl_3{\cdot}6H_2O$), ferrous chloride tetrahydrate ($FeCl_2{\cdot}4H_2O$), ammonium hydroxide (NH_4OH), sodium dodecyl sulfate (SDS), potassium persulfate (KPS), $HAuCl_4{\cdot}3H_2O$ (Sigma), potassium carbonate (K_2CO_3), sodium borohydride ($NaBH_4$), chitosan (CHI, deacetylation degree (DD) > 90%, viscosity average molecular weight (Mv) = 5×10^5 Da), hydroxylamine hydrochloride ($NH_2OH{\cdot}HCl$ 99%), trisodium citrate (Sigma), and styrene (St) and methacrylic acid (MAA) were distilled to remove the inhibitor. All the experimental processes used D.I. water.

2.2. Synthesis of Fe_3O_4 Nanoparticles via Coprecipitation. The MNPs were synthesized via a modified coprecipitation method.[27] Briefly, 24.0 g of $FeCl_3{\cdot}6H_2O$ and 9.8 g of $FeCl_2{\cdot}4H_2O$ was dissolved in 100 mL of D.I. H_2O under the protection of N_2 atm at 80 °C. Under vigorous stirring, 50 mL of $NH_3{\cdot}H_2O$ was quickly injected to the reaction mixture. Immediately, the reaction mixture turned to a black precipitate. 3.76 g of OA was added after 30 min, and it kept reacting for 1.5 h. The as-prepared Fe_3O_4 nanoparticles were collected by a magnet and then washed by ethanol and water for three times, respectively. Then, they were dried at 70 °C in an oven.

2.3. Preparation of Fe_3O_4@P(St/MAA) by Miniemulsion Polymerization. 0.5 g of Fe_3O_4 modified by oleic acid was dispersed in 0.25 g of octane for ultrasounding 5 min in a beaker, and then, 1.8 mL of St and 0.2 mL of MAA were added for ultrasounding another 5 min; the oil phase was formed. Then, the oil phase was dropped to a three-neck flask under mechanical agitation together with the water phase containing 0.04 g of SDS, 48 mL of water, and 0.06 g of KPS. The mixtures were ultrasonicated for 3 min to form a miniemulsion and then reacted for 20 h under N_2 atmosphere at 70 °C. After the polymerization process, the resulting reaction mixture was separated by a permanent magnet in water for three times. Then, we got the resultant Fe_3O_4@P(St/MAA) power by freeze-drying.

2.4. Synthesis of Gold Magnetic Nanoparticles (GMNs). In a typical procedure, there are main four steps to form gold magnetic nanoparticles (GMNs). First, Fe_3O_4@P(St/MAA) was modified with CHI. 0.05 g of Fe_3O_4@P(St/MAA) power was dispersed in 30 mL of 0.2 M acetate buffer (pH 3.5). Then, 1 mL of 1% acetic acid (containing 0.1% CHI) was added by ultrasonics for 15 min. The uncoated CHI was removed and washed three times by a magnet. The Fe_3O_4@P(St/MAA)@CHI precipitation was dispersed with 2 mL of D.I. water. Second, the gold colloids were prepared as in the following method: 20 mL of 0.25 mM $HAuCl_4$ was mixed with 0.25 mM trisodium citrate aqueous solution at 4 °C. Later, 1 mL of fresh 0.08 M $NaBH_4$ solution was quickly added into the mixture with vigorous stirring. Third, to attach gold colloids onto Fe_3O_4@P(St/MAA)@CHI, 2 mL of prepared Fe_3O_4@P(St/MAA)@CHI solution and 20 mL of gold colloids were mixed by ultrasonics for 30 min, forming the Fe_3O_4@P(St/MAA)@CHI@Au_{seed} solution. At last, the gold nanoshells were formed by a seed growth method: 1 mM $HAuCl_4$ was added into 0.25 mg mL^{-1} K_2CO_3. Then, 2 mL of Fe_3O_4@P(St/MAA)@CHI@Au_{seed} was added into the above solution while vigorously stirring. Then, 10 μL (0.36 mmol) of hydroxylamine hydrochloride was diluted with 10 mL of water and pumped. The resulted Fe_3O_4@P(St/MAA)@CHI@Au nanoparticles were washed with water by a permanent magnet for three times, obtaining the GMNs.

2.5. Cytotoxicity Assay. L929 and Hep G2 cells were maintained in Dulbecco's modified Eagle's medium (DMEM) with 10% fetal bovine serum (FBS) and 100 units mL^{-1} penicillin and 100 mg mL^{-1} streptomycin in a humidified atmosphere containing 5% CO_2 at 37 °C. The cytotoxicity of GMNs against L929 and Hep G2 cells was determined with a WST-1 kit with standard protocol.[28] All experiments were carried out for four replicates.

2.6. Dark Field Imaging of GMNs in Cells. A final concentration of 200 μg mL^{-1}GMNs was added to the Hep G2 cells and coincubated for 4 h. Then, the cells were washed with PBS for five times. The dark field imaging was recorded using an inverted fluorescence microscopy (Nikon Eclipse Ti−S, CCD:Ri1) observation with a highly numerical dark field condenser. The scattered light of the samples was collected by an oil objective.

2.7. Hemolytic Behavior of GMNs. Ethylenediaminetetraacetic acid (EDTA)-stabilized rabbit blood was centrifugated to get RBCs. RBCs were diluted 50-fold. 0.5 mL of RBC suspensions were added to 0.5 mL of GMNs suspended in PBS. D.I. water was used as the positive control, and PBS was the negative control. All the sample tubes were mixed mildly and then kept in static condition at room temperature for 3 h. The absorbance of the supernatants was determined at 570 nm. The percentage of hemolysis was calculated by: hemolysis % = (sample absorbance − negative control absorbance)/(positive control absorbance − negative control absorbance) × 100.[29]

2.8. General Analysis. The prepared particles were characterized by a transmission electron microscope (JEM-2100) operating at 200 kV. A D8 Focus XRD system (Bruker) was used for powder X-ray diffraction (XRD) measurements. UV/vis/NIR spectra were recorded by a spectrophotometer (JASCO V-570). Infrared spectroscopy was recorded on a Spectrum One Excalibur 3100 FTIR spectrometer. Magnetism was measured by vibrating a sample magnetometer (VSM). The naoparticles size and zeta potential were measured by a Malvern Zetasizer 3000HS. The MRI was measured by a Philips Achieva 3.0T TX MRI Scanner.

3. RESULTS AND DISCUSSION

Figure 1a shows the preparation method and possible formation mechanism of GMNs nanoparticles. Briefly, the Fe_3O_4 nanoparticles (Figure S1, Supporting Information) of about 10 nm were synthesized by the coprecipitation method and modified with OA. Then, OA-modified Fe_3O_4 was embedded in the polymer matrix by the miniemulsion polymerization. As the MAA monomer was used, their surface had abundant COO^- groups, making the surface of the nanoparticles with negative charge (Figure 1b), and the zeta potential was −22 mV (see Table 1). The addition of CHI after the synthesis of Fe_3O_4@P(St/MAA) was found to be an effective method of controlling the surface charge of Fe_3O_4@P(St/MAA) because CHI with amine groups can reverse the negatively charged Fe_3O_4@P(St/MAA) to positive charge. As shown in Table 1, the ζ potential of Fe_3O_4@P(St/MAA)@CHI nanoparticles was +3.3 mV. In addition, it can be clearly observed from the TEM image (Figure 1c) that the surface of particles became blurry because of coating of CHI. The obtained nanoparticles with positively charged surface made them favorable for electrostatic attachment with negatively

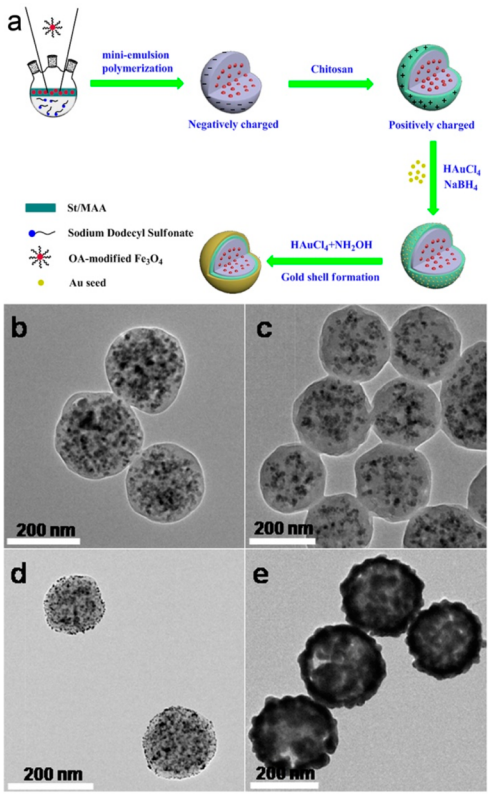

Figure 1. (a) Schematic diagram for the preparation of GMNs core/shell nanostructure. TEM images of (b) Fe_3O_4 @P(St/MAA), (c) Fe_3O_4 @P(St/MAA)@CHI, (d) Fe_3O_4 @P(St/MAA)@CHI@Au_{seed}, and (e) GMNs.

Table 1. Size and Zeta Potential of Different Nanoparticles Measured by a Malvern Zetasizer 3000HS

particles type	size/nm	zeta potential/mv
Fe_3O_4@P(St/MAA)	287.7 ± 0.9	−22.1 ± 1.3
Fe_3O_4@P(St/MAA)@CHI	295.0 ± 2.7	3.3 ± 0.3
Fe_3O_4@P(St/MAA)@CHI@Au_{seed}	305.3 ± 2.4	−25.8 ± 2.0
GMNs	335.8 ± 2.9	−28.2 ± 0.4

charged gold colloids. As observed in Figure 1d, the gold colloids could be obviously seen on the Fe_3O_4@P(St/MAA)@CHI nanoparticles surface. After the adsorption of gold colloids, the gold nanoshells were formed through reduction of chloroauric acid ($HAuCl_4 \cdot 3H_2O$) using hydroxylamine hydrochloride ($NH_2OH \cdot HCl$) as a reducing agent by the seed growth method. From Figure 1e, we can see compact gold nanoshells coating the nanoparticles, forming a ∼30 nm thick gold layer, which is thick enough to observe the characteristic surface plasmon bands in the NIR spectra.[30,31]

To get compact gold nanoshells, there are three critical factors. First, it is important to synthesize small gold colloids for attaching onto the Fe_3O_4@P(St/MAA)@CHI nanoparticles. The gold colloids were prepared by the citrate and $NaBH_4$ reducing method. The $NaBH_4$ is a strong reducing agent which could quickly reduce the $HAuCl_4$ to obtain small gold nanoparticles. Meanwhile, citrate acts as both weak reducing agent and stabilizing agent, making the surface of gold nanoparticles negatively charged.[32] Second, it is critical to control the formation of new nucleation in the gold nanoshells growth step. The potassium carbonate used mainly provides OH^- to coordinate with $HAuCl_4$. It is known that the $HAuCl_4$ has various coordination compounds at different pH values, which affects the formation of compact gold nanoshells.[33] At pH 10, the coordination compound of $HAuCl_4$ is stable $[Au(OH)_4]^-$. The self- nucleation would be inhibited, while the present gold nuclei could grow larger to form compact gold nanoshells. At last, a proper reduction agent should be chosen to control the rate of reducing reaction.[34] In this course, a weak reducing agent, hydroxylamine hydrochloride, was chosen to adjust the reaction rate of gold, which is helpful to form compact gold naoshells.[35]

Figure 2A shows the XRD patterns of the obtained Fe_3O_4, Fe_3O_4@P(St/MAA), and GMNs. The diffraction peak

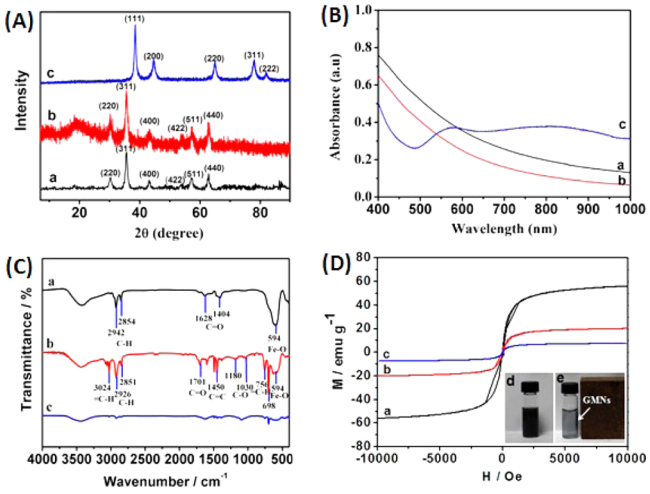

Figure 2. (A) XRD patterns of (a) OA modified Fe_3O_4, (b) Fe_3O_4 @P(St/MAA), and (c) GMNs. (B) UV/vis/NIR spectra of (a) Fe_3O_4@P(St/MAA), (b) Fe_3O_4@P(St/MAA)@CHI@Au_{seed}, and (c) GMNs. (C) FTIR spectra of (a) Fe_3O_4 nanoparticles, (b) Fe_3O_4@P(St/MAA), and (c) GMNs. (D) Hysteresis loops of (a) Fe_3O_4, (b) Fe_3O_4 @P(St/MAA), and (c) GMNs. Photos of the GMNs solution (d) before and (e) after being separated by a magnet. The arrow pointed to the GMNs moved aside by a magnet.

positions at 30.22°, 35.60°, 43.05°, 53.64°, 57.10°, and 62.85° could be attributed to the (220), (311), (400), (422), (511), and (440) planes of Fe_3O_4, respectively.[36] In Figure 2A b, clearly, the XRD peaks for Fe_3O_4@P(St/MAA) nanoparticles (Figure 2A b) are similar to that of Fe_3O_4 nanoparticles capped with oleic acid (Figure 2A a). Except the peaks of Fe_3O_4, the broad peaks at 20−30° were also observed (Figure 2A b), revealing that Fe_3O_4 was coated in the polymer. The diffraction peak positions of GMNs at 38.49°, 44.47°, 64.93°, 77.90°, and 81.80° could be attributed to (111), (200), (220), (311), and (222) planes of Au, respectively. Clearly, the characteristic peaks of Fe_3O_4 no longer appear in the final material (Figure 2A c). The absence of diffraction peaks for Fe_3O_4 is possible because of the heavy atom effect of gold. It provides a further indication that gold nanoshells have been coated on the Fe_3O_4@P(St/MAA)@CHI and the thickness is at least 2.5 nm.[31] The fact indicates the formation of GMNs core/shell structure.

Figure 2B shows the UV/vis/NIR absorption spectra of Fe_3O_4@P(St/MAA), Fe_3O_4 @P(St/MAA)@CHI@Au_{seed}, and GMNs. From Figure 2B a and b, there are not any obvious absorbance peaks of Fe_3O_4@P(St/MAA) or Fe_3O_4@P(St/MAA)@CHI@Au_{seed}. However, the GMNs shows a clear SPR characteristic peak at 800 nm (Figure 2B c). This is the

dx.doi.org/10.1021/am400721s | ACS Appl. Mater. Interfaces 2013, 5, 4966−4971

characteristic absorption property of gold nanoshells, indicating that gold nanoshells structure has been successfully formed.

To confirm that Fe_3O_4 nanoparticles were embedded in the carboxylated polymer, the FTIR spectra of the prepared OA-modified Fe_3O_4, Fe_3O_4@P(St/MAA), and GMNs were measured (Figure 2C). For OA-modified Fe_3O_4 (Figure 2C a), the characteristic peaks of 594, 2854, and 2942 cm^{-1} were, respectively, contributed to the Fe−O vibration and the CH_3 and the CH_2 stretching vibrations. The two peaks of 1628 and 1406 cm^{-1} were related to antisymmetric vibration of COO^- group and symmetric vibration of COO^- group, respectively,[37] indicating that Fe_3O_4 nanoparticles were successfully modified with OA. Fe_3O_4@P(St/MAA) (Figure 2C b) shows the peak of Fe−O at 594 cm^{-1}. In addition, different from the OA modified Fe_3O_4, new peaks appeared at 1701 cm^{-1} (stretching vibration of C═O), 1180 and 1030 cm^{-1}(stretching vibration of C−O), 756 and 698 cm^{-1} (═C−H of benzene ring), and 1450 cm^{-1}(asymmetric vibration of C═C of benzene ring). It shows that magnetic Fe_3O_4 was completely embedded in carboxylated polymer via the miniemulsion polymerization method. When Fe_3O_4@P(St/MAA) was coated with gold nanoshells, the peaks of GMNs decreased (Figure 2C c), attributed to the different electron density between Au and Fe_3O_4@P(St/MAA).[36] With Au as the electron density donator, the gold nanoshells can shield an electron cloud of Fe_3O_4@P(St/MAA), resulting in the decreased intensity of the characteristic peaks of Fe_3O_4@P(St/MAA). Generally, the FTIR spectra showed that OA-modified, Fe_3O_4@P(St/MAA) and GMNs have been successfully prepared.

The magnetic properties of Fe_3O_4, Fe_3O_4@P(St/MAA), and GMNs nanoparticles were investigated by a vibrating sample magnetometer (VSM) at room temperature. From Figure 2D, the saturation magnetization values for Fe_3O_4, Fe_3O_4@P(St/MAA), and GMNs were 56.0, 20.1, and 7.5 emu/g, respectively. The saturation magnetization values gradually decreased with the increased number of coating layers on Fe_3O_4 nanoparticles; Fe_3O_4@P(St/MAA) and GMNs declined as the number of coatings increased, mainly owing to the decrease of Fe_3O_4 content and the diamagnetic property of the gold nanoshells.[38] Although saturation magnetization is relatively low, GMNs could still be easily attracted aside by a magnet (Figure 2D e).

To demontrate the T 2 enhancing capability in vitro, the GMNs of different concentrations were measured by the T 2-weighted MRI using a Philips Achieva 3.0T clinical MRI system. The equivalent concentrations of GMNs were 2.5, 5, 15, 25, and 50 $\mu g\ mL^{-1}$ of Fe (quantitatively measured using ICP-AES), using water as a control. We can see from Figure 3A

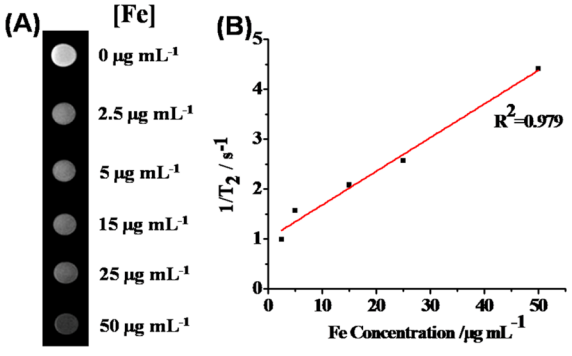

Figure 3. (A) T_2 weighted MR images of GMNs; (B) T_2 relaxation rate $(1/T_2)$ as a function of Fe concentration ($\mu g\ mL^{-1}$).

that an obvious darkening of T 2-weighted MRI was observed with the increasing concentration of Fe. As shown in Figure 3B, it was shown that the T_2 relaxation rate $(1/T_2)$ increased with the increase of the concentrations of Fe, showing a linear relationship. The results indicate the GMNs can elevate the T_2 relaxation rate, which make them useful as MRI contrast agents.

Owing to the unique plasmon resonance and light scattering properties, gold nanoparticles have been widely used in biomedical imaging.[39] To confirm that the GMNs could act as a DFI contrast agent, the cellular imaging was carried out. As shown in Figure 4, the cellular uptake of nanoparticles and dark

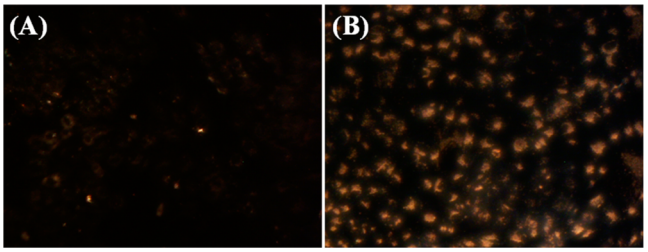

Figure 4. Dark field images of (A) Hep G2 cells without GMNs and (B) Hep G2 cells after incubation with GMNs.

field imaging of the Hep G2 were investigated. In the control cells without GMNs, most of the cells were dark (Figure 4A). Only a small portion of cells showed very dim light signals because of the scattered light and autofluorescence of the cells.[14,40] After cellular uptake of GMNs, their morphology of the Hep G2 cells kept intact. The cells were lit up in the dark field with orange colorful spots, owing to the light scattering of gold nanoshells (Figure 4B). From these data, we conclude that the GMNs could act as a good DFI contrast agent.

To further prove the photothermal effect of GMNs, monitoring the temperature of 0.5 mL of GMNs aqueous solution with various concentrations (0, 2.5, 5, 15, 25, and 50 $\mu g\ mL^{-1}$ Fe) irradiated by a NIR laser (808 nm, 1 W cm^{-2}) was investigated. As shown in Figure 5A, the solution of GMNs (50 $\mu g\ mL^{-1}$) dispersed in water when exposed to the NIR laser light for 10 min; the solution temperature was elevated from 31.33 to 59.05 °C. In comparison, the temperature of the water in the absence of GMNs increased only 4.15 °C. The magnitude of temperature elevation increased with the increased concentration of GMNs. These data indicated that GMNs could act as an efficient photothermal coupling agent. To evaluate the hyperthermia efficacy of GMNs in vitro of different concentrations under NIR light irradiation, the viability of Hep G2 and L929 cells was determined using the WST-1 assay. Hep G2 and L929 cells were incubated in DMEM (high glucose) with 10% fetal bovine serum (BSA) with different concentrations of GMNs at 37 °C for 24 h. Each group was irradiated by NIR light (1W cm^{-2}, 3 min). After the cells were incubated at 37 °C for another 24 h, 20 μL of WST-1 solution was added; then, the inhibition rates were measured at 450 nm on a microplate reader. Data were presented as a mean standard deviation (SD) of at least four independent experiments. As shown in Figure 5B of hyperthermia therapy, with the increase of concentration of GMNs, the cytotoxicity against Hep G2 and L929 cells increased with a dose-dependent behavior. At 100 $\mu g\ mL^{-1}$ of GMNs concentration, the inhibition rate is 82.4%, demonstrating great potential as a NIR absorbing agent in photothermal therapy.

dx.doi.org/10.1021/am400721s | ACS Appl. Mater. Interfaces 2013, 5, 4966−4971

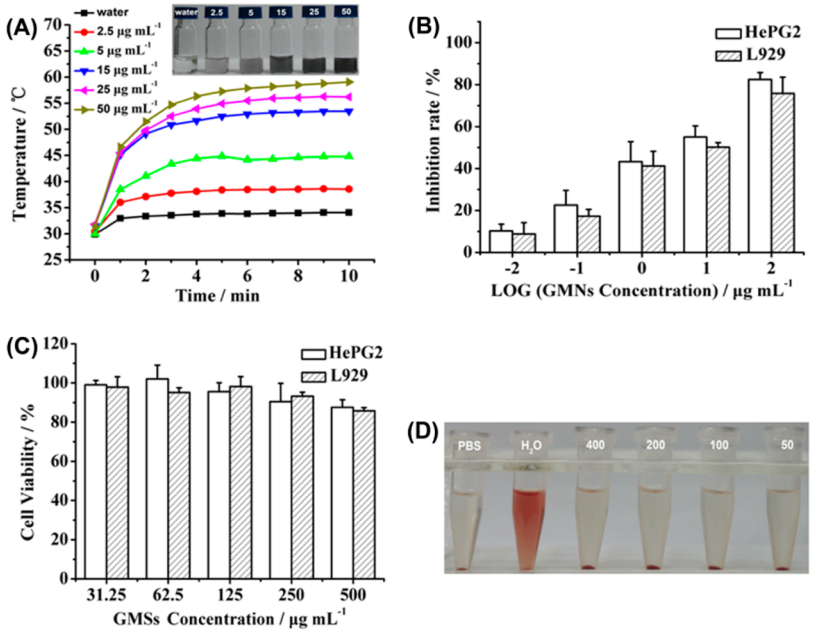

Figure 5. (A) Photothermal effect of pure water and GMNs with different concentrations upon the irradiation of 1 W cm^{-2} at 808 nm laser (the inset photograph shows various concentrations of GMNs dispersed in water). (B) Inhibition rate of GMNs for 24 h as a function of GMNs concentration; Hep G2 and L929 cells were irradiated with NIR light (1 W cm^{-2} for 3 min). (C) The viability of Hep G2 and L929 cells with different concentrations of GMNs. (D) Hemolysis for GMNs, using PBS as negative control and D.I. water as a positive control; the GMNs are suspended in RBCs suspensions with different concentrations (right four tubes).

To investigate the biocompatibility is important for clinical application of GMNs. We evaluated cytotoxicity of GMNs on Hep G2 and L 929 cells by the WST-1 viability assay after 24 h incubation. At the highest tested concentration of 500 μg mL^{-1}, as seen from Figure 5C, the GMNs cell viability is more than 85.7%, demonstrating that the GMNs have no obvious cytotoxicity to Hep G2 and L929 cells.

The hemolytic behavior of various concentrations of GMNs with rabbit red blood cells (RBCs) was also investigated. EDTA-stabilized rabbit blood was centrifugated and washed with PBS to harvest RBCs. Herein, water was used as the positive controls and PBS was the negative control. All the sample tubes were mixed mildly and kept for 3 h at room temperature. The absorbance of the released hemoglobin in the supernatant was measured at 450 nm using a microplate reader. The hemolysis of RBCs with GMNs even at the concentration as high as 400 μg mL^{-1} was lower than 5% (data not shown) (Figure 5D), indicating their excellent blood compatibility. Therefore, we can conclude that GMNs have good biocompatibility.

4. CONCLUSIONS

In conclusion, we have developed a facile strategy to synthesize Fe_3O_4@P(St/MAA)@Chitosan@Au nanoparticles. In comparison with the previous method, where gold nanoshells were directly coated on Fe_3O_4 or Fe_3O_4/SiO_2 composites, our nanoparticles are embedded in a dielectric polymer matrix. We synthesize monodispersed Fe_3O_4@P(St/MAA) nanoparticles though the miniemulsion polymerization. This strategy could protect the Fe_3O_4 from aggregation and also control the nanoparticle size and magnetic and optical properties. Then, the gold nanoshells were formed via the seed growth method, using CHI as the middle layer. The resulting nanoparticles used the CHI as the middle layer, which has a good biocompatibility through the standard WST-1 assay on the Hep G2 and L929 cells. Moreover, the obtained multifunctional nanoparticles had a low hemolyticity. We also demonstrate that the structure of magnetic Fe_3O_4 core covered with gold nanoshells can be used for MRI, simultaneously in dark field imaging. The excellent photothermal property of GMNs allows them to be good agents for photothermal tumor therapy. Further studies of targeted delivery and photothermal effect for in vivo application are under investigation.

■ ASSOCIATED CONTENT

Ⓢ Supporting Information

TEM image of OA coated iron oxide nanoparticles. This material is available free of charge via the Internet at http://pubs.acs.org.

■ AUTHOR INFORMATION

Corresponding Author

*Tel: +86-10-82543521. E-mail: rj@mail.ipc.ac.cn (J.R.), tangfq@mail.ipc.ac.cn (F.T.).

Author Contributions

The manuscript was written through contributions of all authors. All authors have given approval to the final version of the manuscript.

Notes

The authors declare no competing financial interest.

■ ACKNOWLEDGMENTS

This work was supported by the National Natural Science Foundation of China (No. 81171454, 31271075, 81000667, 81201814) and Beijing Nova Program (Z111103054511113).

■ REFERENCES

(1) Hao, R.; Xing, R. J.; Xu, Z. C.; Hou, Y. L.; Gao, S.; Sun, S. H. *Adv. Mater.* **2010**, *22*, 2729−2742.

(2) Liu, J.; Qiao, S. Z.; Hu, Q. H.; Lu, G. Q. *Small* **2011**, *7*, 425−443.
(3) Yang, C.; Wu, J. J.; Hou, Y. L. *Chem. Commun.* **2011**, *47*, 5130−5141.
(4) Kumar, C. S.; Mohammad, F. *Adv. Drug Delivery Rev.* **2011**, *63*, 789−808.
(5) Zhao, Q.; Wang, L. N.; Cheng, R.; Mao, L. D.; Arnold, R. D.; Howerth, E. W.; Chen, Z. G.; Platt, S. *Theranostics* **2012**, *2*, 113−121.
(6) Reddy, L. H.; Arias, J. L.; Nicolas, J.; Couvreur, P. *Chem. Rev.* **2012**, *112*, 5818−5878.
(7) Mahmoudi, M.; Hosseinkhani, H.; Hosseinkhani, M.; Boutry, S.; Simchi, A.; Journeay, W. S.; Subramani, K.; Laurent, S. *Chem. Rev.* **2011**, *111*, 253−280.
(8) Lee, J. E.; Kim, H.; Kim, J.; Choi, S. H.; Kim, J. H.; Kim, T.; Song, I. C.; Park, S. P.; Moon, W. K.; Hyeon, T. *J. Am. Chem. Soc.* **2010**, *132*, 552−557.
(9) Shen, J.; Sun, L. D.; Zhang, Y. W.; Yan, C. H. *Chem. Commun.* **2010**, *46*, 5731−5733.
(10) Shi, D. L.; Cho, H. S.; Chen, Y.; Xu, H.; Gu, H. C.; Lian, J.; Wang, W.; Liu, G. K.; Huth, C.; Wang, L. M.; Ewing, R. C.; Budko, S.; Pauletti, G. M.; Dong, Z. Y. *Adv. Mater.* **2009**, *21*, 2170−2173.
(11) Levin, C. S.; Hofmann, C.; Ali, T. A.; Kelly, A. T.; Morosan, E.; Nordlander, P.; Whitmire, K. H.; Halas, N. J. *ACS Nano* **2009**, *3*, 1379−1388.
(12) Cheng, L.; Yang, K.; Li, Y.; Zeng, X.; Shao, M. W; Lee, S. T.; Liu, Z. *Biomaterials* **2012**, *33*, 2215−2222.
(13) Cheng, L.; Yang, K.; Li, Y.; Chen, J.; Wang, C.; Shao, M.; Lee, S.-T.; Liu, Z. *Angew. Chem., Int. Ed.* **2011**, *50*, 7385−7390.
(14) Wax, A.; Sokolov, K. *Laser Photonics Rev.* **2009**, *3*, 146−158.
(15) Liu, H. Y.; Chen, D.; Li, L. L.; Liu, T. L.; Tan, L. F.; Wu, X. L.; Tang, F. Q. *Angew. Chem., Int. Ed.* **2011**, *50*, 891−895.
(16) Liu, H. Y.; Liu, T. L.; Li, L. L.; Hao, N. J.; Tan, L. F.; Meng, X. W.; Ren, J.; Chen, D.; Tang, F. Q. *Nanoscale* **2012**, *4*, 3523−3529.
(17) Liu, H. Y.; Liu, T. L.; Wu, X. L.; Li, L. L.; Tan, L. F.; Chen, D.; Tang, F. Q. *Adv. Mater.* **2012**, *24*, 755−761.
(18) Narayanan, S.; Sathy, B. N.; Mony, U.; Koyakutty, M.; Nair, S. V.; Menon, D. *ACS Appl. Mater. Interfaces* **2012**, *4*, 251−260.
(19) Wang, L. Y.; Park, H. Y.; Lim, S. I. I.; Schadt, M. J.; Mott, D.; Luo, J.; Wang, X.; Zhong, C. J. *J. Mater. Chem.* **2008**, *18*, 2629−2635.
(20) Dong, W. J.; Li, Y. S.; Niu, D. C.; Ma, Z.; Gu, J. L.; Chen, Y.; Zhao, W. R.; Liu, X. H.; Liu, C. S.; Shi, J. L. *Adv. Mater.* **2011**, *23*, 5392−5397.
(21) Bardhan, R.; Chen, W.; Bartels, M.; Perez-Torres, C.; Botero, M. F.; McAninch, R. W.; Contreras, A.; Schiff, R.; Pautler, R. G.; Halas, N. J.; Joshi, A. *Nano Lett.* **2010**, *10*, 4920−4928.
(22) Wang, L. Y.; Bai, J. W.; Li, Y. J.; Huang, Y. *Angew. Chem., Int. Ed.* **2008**, *47*, 2439−2442.
(23) Hsiao, S. C.; Ou, J. L.; Sung, Y.; Chang, C. P.; Ger, M. D. *Colloid Polym. Sci.* **2010**, *288*, 787−794.
(24) Liu, H. Y.; Chen, D.; Tang, F. Q.; Du, G. J.; Li, L. L.; Meng, X. W.; Liang, W.; Zhang, Y. D.; Teng, X.; Li, Y. *Nanotechnology* **2008**, *19*, 455101.
(25) Bae, K. H.; Park, M.; Do, M. J.; Lee, N.; Ryu, J. H.; Kim, G. W.; Kim, C.; Park, T. G.; Hyeon, T. *ACS Nano* **2012**, *6*, 5266−5273.
(26) Huang, H. Z.; Yang, X. R. *Biomacromolecules* **2004**, *5*, 2340−2346.
(27) Xu, H.; Cui, L. L.; Tong, N. H.; Gu, H. C. *J. Am. Chem. Soc.* **2006**, *128*, 15582−15583.
(28) Wang, J.; Chen, B.; Chen, J.; Cai, X.; Xia, G.; Liu, R.; Chen, P.; Zhang, Y.; Wang, X. *Int. J. Nanomed.* **2011**, *6*, 203−211.
(29) Zhao, Y. N.; Sun, X. X.; Zhang, G. N.; Trewyn, B. G.; Slowing, I. I.; Lin, V. S. Y. *ACS Nano* **2011**, *5*, 1366−1375.
(30) Smolensky, E. D.; Neary, M. C.; Zhou, Y.; Berquo, T. S.; Pierre, V. C. *Chem.Commun.* **2011**, *47*, 2149−2151.
(31) Xu, Z. C.; Hou, Y. L.; Sun, S. H. *J. Am. Chem. Soc.* **2007**, *129*, 8698−8699.
(32) Jana, N. R.; Gearheart, L.; Murphy, C. J. *Langmuir* **2001**, *17*, 6782−6786.
(33) Phonthammachai, N.; Kah, J. C. Y.; Jun, G.; Sheppard, C. J. R.; Olivo, M. C.; Mhaisalkar, S. G.; White, T. J. *Langmuir* **2008**, *24*, 5109−5112.
(34) Graf, C.; van Blaaderen, A. *Langmuir* **2002**, *18*, 524−534.
(35) Duff, D. G.; Baiker, A.; Gameson, I.; Edwards, P. P. *Langmuir* **1993**, *9*, 2310−2317.
(36) Zhang, H.; Zhong, X.; Xu, J. J.; Chen, H, Y. *Langmuir* **2008**, *24*, 13748−13752.
(37) Xuan, S.; Wang, Y. X.; Yu, J. C.; Leung, K. C. *Langmuir* **2009**, *25*, 11835−11843.
(38) Wu, Y. P.; Zhang, T.; Zheng, Z. H.; Ding, X. B.; Peng, Y. X. *Mater. Res. Bull.* **2010**, *45*, 513−517.
(39) Hu, Y.; Chen, Q.; Ding, Y.; Li, R. T.; Jiang, X. Q.; Liu, B. R. *Adv. Mater.* **2009**, *21*, 3639−3643.
(40) El-Sayed, I. H.; Huang, X. H.; El-Sayed, M. A. *Nano Lett.* **2005**, *5*, 829−834.